Magnetic properties of the low-dimensional $BaM_2Si_2O_7$ system (M = Cu, Co, Mn)

G. H. Wang,[1] C. Y. Xu,[1] H. B. Cao,[2] T. Hong,[2] Q. Huang,[3] Q. Y. Ren,[1] J. Q. Xu,[1] H. D. Zhou,[1,3] W. Luo,[1,4,5,*] D. Qian,[1,5] and J. Ma[1,5,†]

[1]*Key Laboratory of Artificial Structures and Quantum Control, School of Physics and Astronomy, Shanghai Jiao Tong University, Shanghai 200240, China*

[2]*Neutron Scattering Division, Oak Ridge National Laboratory, Oak Ridge, Tennessee 37831, USA*

[3]*Department of Physics and Astronomy, University of Tennessee, Knoxville, Tennessee 37996-1200, USA*

[4]*Institute of Natural Sciences, Shanghai Jiao Tong University, Shanghai 200240, China*

[5]*Collaborative Innovation Center of Advanced Microstructures, Nanjing 210093, China*

(Received 29 July 2018; revised manuscript received 25 June 2019; published 26 July 2019)

We investigated the magnetic properties of the low-dimensional $BaM_2Si_2O_7$ (M = Cu, Co, and Mn) system using both experimental measurements and theoretical calculations. Magnetization, specific heat, and single crystal neutron diffraction measurements have been performed on single crystal $BaMn_2Si_2O_7$. The spin structure was determined and a magnetic phase diagram with applied field along the b axis was constructed, which contains a spin flop transition around 6 T. Magnetization and specific heat measurements confirmed the presence of weak ferromagnetism in $BaCo_2Si_2O_7$. Furthermore, we performed local-spin density approximation with on-site Coulomb energy (LSDA + U) calculations for the $BaM_2Si_2O_7$ (M = Cu, Co, and Mn) system. Based on the first-principles calculations, the origin of the magnetic differences of the three materials is discussed.

DOI: 10.1103/PhysRevB.100.035131

I. INTRODUCTION

Unlike traditional one-dimensional (1D) and three-dimensional (3D) magnetic systems, a quasi-1D magnetic material has unique magnetic properties. If the magnetic moment is as small as 1/2 or 1, the quantum effect as spin/thermal fluctuation could interfere with the ground state and complicate the system: the magnetic order could not form even at 0 K in a purely 1D spin-1/2 chain system, while the interchain interactions could induce a Néel ordering state as a 3D antiferromagnet [1–4]. As a result, a quasi-1D system with weak coupling between the magnetic chains will exhibit a crossover from 1D magnetic behavior [5–10] at high temperatures to a 3D ordered state at low temperatures. Moreover, the strong spin anisotropy of the system could exhibit a rich magnetic phase diagram under applied magnetic field below the ordering temperature. Hence studying the inter- and intralayer interaction of the quasi-1D system with different momentum is very important and has received considerable attention in the past years.

$BaM_2Si_2O_7$ (M = Cu, Co, and Mn) with layered structure is an excellent system to study such low-dimensional magnetic behavior. Among these three compounds, $BaCu_2Si_2O_7$, which has a spin 1/2 (Cu^{2+}) feature, has been extensively studied. This compound adopts an orthorhombic structure with a space group of *Pnma*. The nearest Cu^{2+} ions through the O^{2-} ions construct a zigzag chain along the c axis. Below $T_N = 9.2$ K, an antiferromagnetic ordered state is formed, in which the magnetic easy axis is the c axis [11]. With applied magnetic field along the c axis, a two step spin-flop transition has been reported [12–15]. Moreover, the exchange interactions of the 1D magnetic spin chain have been studied by inelastic neutron scattering measurements and theoretical calculations [16–20].

The replacement of Cu^{2+} ions with larger-sized Co^{2+} and Mn^{2+} ions results in a structural distortion. $BaCo_2Si_2O_7$ and $BaMn_2Si_2O_7$ have a monoclinic crystal structure with the space group $C2/c$ [21]. Accordingly, the M-O ligands for the CuO_4 plaquettes in the Cu sample now form a Co/MnO_4 tetrahedron in the Co and Mn samples [22,23], as shown in Fig. 1. Previous studies, while limited, suggested a ferromagneticlike ground state for $BaCo_2Si_2O_7$ with spin-3/2 (Co^{2+}) [22,24]. For $BaMn_2Si_2O_7$, powder neutron diffraction study demonstrated an antiferromagnetic spin structure along the c axis below $T_N = 26$ K [25]. Magnetization measurements with an applied field along the b axis suggested a spin flop transition at $B = 6$ T. Taking into account these previous studies, it becomes clear that each of the three compositions in the $BaM_2Si_2O_7$ system have distinct magnetic properties.

Due to the limited studies on $BaCo_2Si_2O_7$ and $BaMn_2Si_2O_7$, several questions have been left open. For example, the ground state of $BaCo_2Si_2O_7$ needs to be confirmed by more detailed investigation. In the case of $BaMn_2Si_2O_7$, the magnetic properties and magnetic structure were preliminarily studied using magnetization measurements and powder neutron diffraction in our previous work [25]. Although a spin-flop transition was observed with magnetic field, further studies are necessary to build a complete magnetic phase diagram. Moreover, the spin structure of $BaMn_2Si_2O_7$ was determined using a polycrystalline sample. As such, an investigation utilizing single crystal neutron diffraction, which usually leads to a

*wdluo@sjtu.edu.cn
†jma3@sjtu.edu.cn

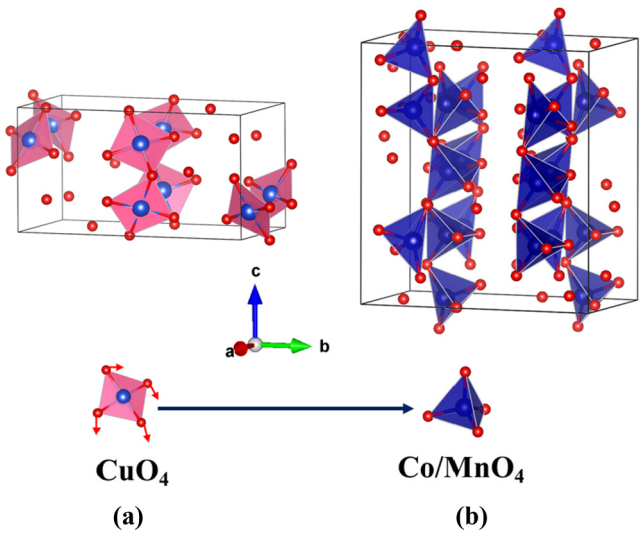

FIG. 1. (a) Schematic crystalline structures for (a) $BaCu_2Si_2O_7$ and (b) $BaM_2Si_2O_7$ (M = Mn and Co).

more accurate determination of spin structure, is deserved. Most importantly, there has been no systematic study on this system to better understand the driving force for the distinct magnetic ground states. In this paper, we (1) performed magnetic properties, specific heat, and single crystal neutron diffraction measurements under applied fields to revisit the spin structure and construct the magnetic phase diagram for single crystalline $BaMn_2Si_2O_7$, (2) studied the physical properties of polycrystalline $BaCo_2Si_2O_7$ to confirm its magnetic ground state, and (3) performed LSDA + U calculations to systematically study the exchange interactions of the system. Our discussions based on the detailed comparison among the obtained exchange interactions for the system show that the structure distortion and the outer shell electronic configuration are two main reasons for the systematic changes of the magnetic ground states for these three samples.

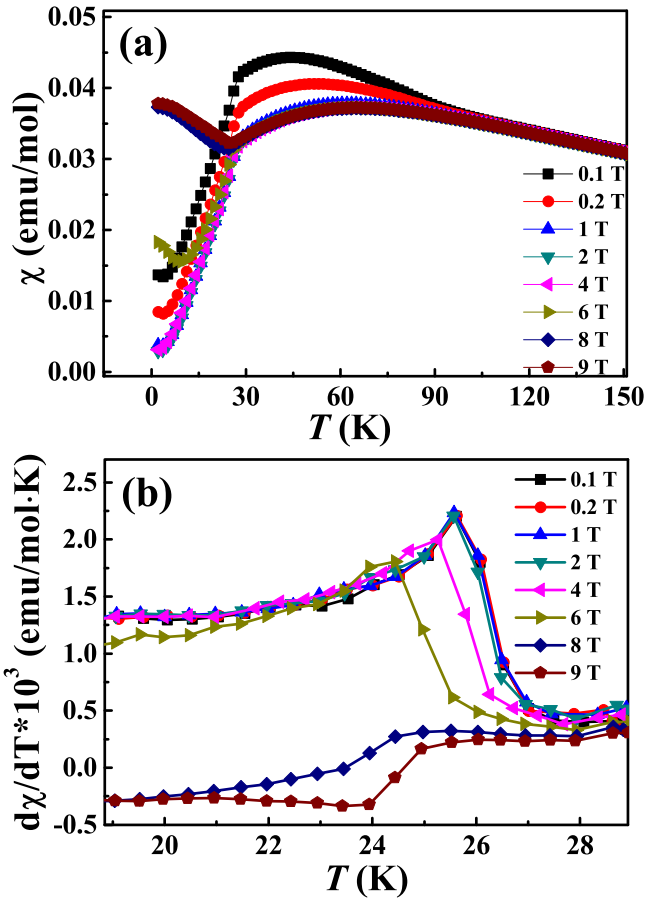

FIG. 2. (a) Temperature dependence of susceptibility (χ) and (b) its derivative $d\chi/dT$ at selected fields for $BaMn_2Si_2O_7$. The applied field is along the b axis.

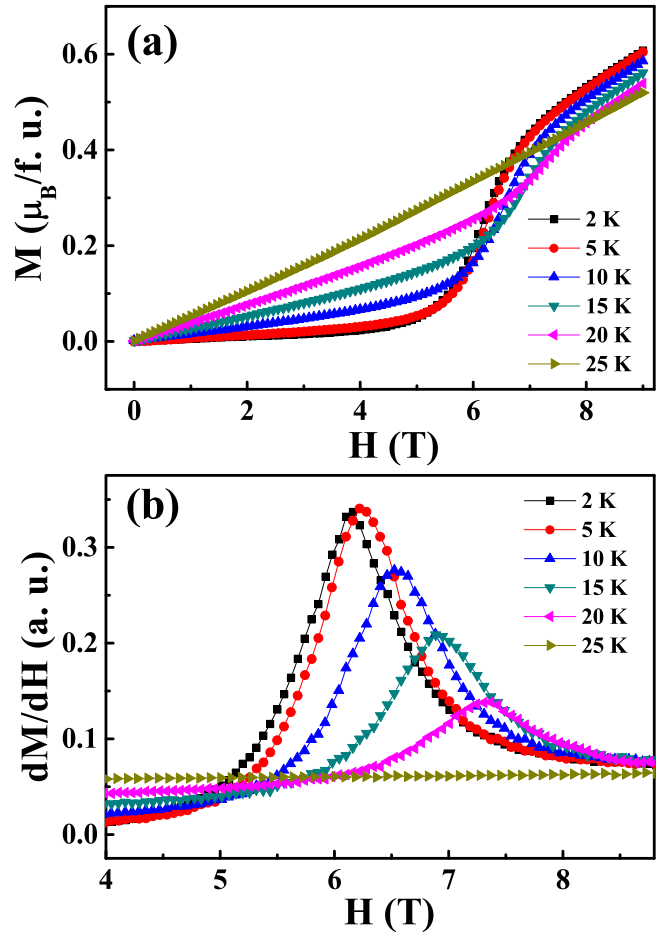

FIG. 3. (a) Field dependence of magnetization (M) and (b) its derivative dM/dH at selected temperatures for $BaMn_2Si_2O_7$. The applied field is along the b axis.

II. EXPERIMENT

Single crystal $BaMn_2Si_2O_7$ was grown using an image furnace. The detailed method is described elsewhere [25]. Polycrystalline $BaCo_2Si_2O_7$ was synthesized by solid state reactions. Stoichiometric mixtures of $BaCO_3$, $CoCO_3$, and SiO_2 were ground and reacted at a temperature of 1100 °C in air for 60 h with several intermediate grindings. The magnetic susceptibility, magnetization, and heat capacity were measured using a PPMS (physical property measurement system,

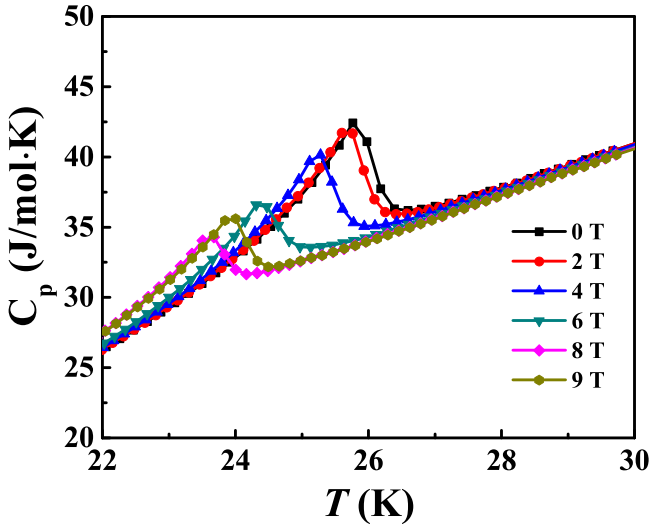

FIG. 4. Temperature dependence of specific heat around the transitions at selected fields for $BaMn_2Si_2O_7$. The applied field is along the b axis.

Quantum Design). The zero field single-crystal neutron diffraction was performed at the HB-3A Four-Circle Diffractometer and high-field neutron diffraction measurements were carried out at the cold neutron triple-axis (CTAX) spectrometer using an 11-Tesla cryomagnet at the High Flux Isotope Reactor, Oak Ridge National Laboratory. A neutron wavelength of 1.005 Å from a bent perfect Si-331 monochromator was used in HB-3A [26]. The neutron diffraction data were refined by the FullProf Suite [27].

III. RESULTS

A. $BaMn_2Si_2O_7$

The temperature dependence of susceptibility, χ, under selected magnetic fields for $BaMn_2Si_2O_7$ is shown in Fig. 2. With an applied field $H = 0.1$ T along the b axis, χ shows a broad peak around 30–40 K, that is followed by a sharp decline around 26 K, which suggests that $BaMn_2Si_2O_7$ undergoes a transition from the 1D Bonner-Fisher model [6,28] (broad peak) to long-range magnetic order (sharp drop). The ordering temperature, $T_N = 26$ K for 0.1 T, is defined as the peak position of the derivative of χ, Fig. 2(b). For $H \leqslant 6$ T, T_N decreases with increasing magnetic field; for $H \geqslant 8$ T, T_N increases with increasing magnetic field, and χ increases with decreasing temperature below T_N. This distinct behavior between different field regimes suggests a spin flop transition induced by an applied field of $6 \sim 8$ T.

The field dependence of magnetization, M, at selected temperatures for $BaMn_2Si_2O_7$ is shown in Fig. 3. With H along the b axis and temperatures below T_N, M exhibits a sharp slope change around 6 T. Accordingly, the dM/dH curve [Fig. 3(b)] shows a sharp peak, which defines the critical field, H_c. At 2 K, $H_c = 6.0$ T and shifts to higher fields with increasing temperature. As the temperature approaches T_N, (e.g., 25 K), this increase becomes very weak.

The specific heat for $BaMn_2Si_2O_7$ is shown in Fig. 4. At zero field, the sharp peak at 26 K corresponds to the T_N.

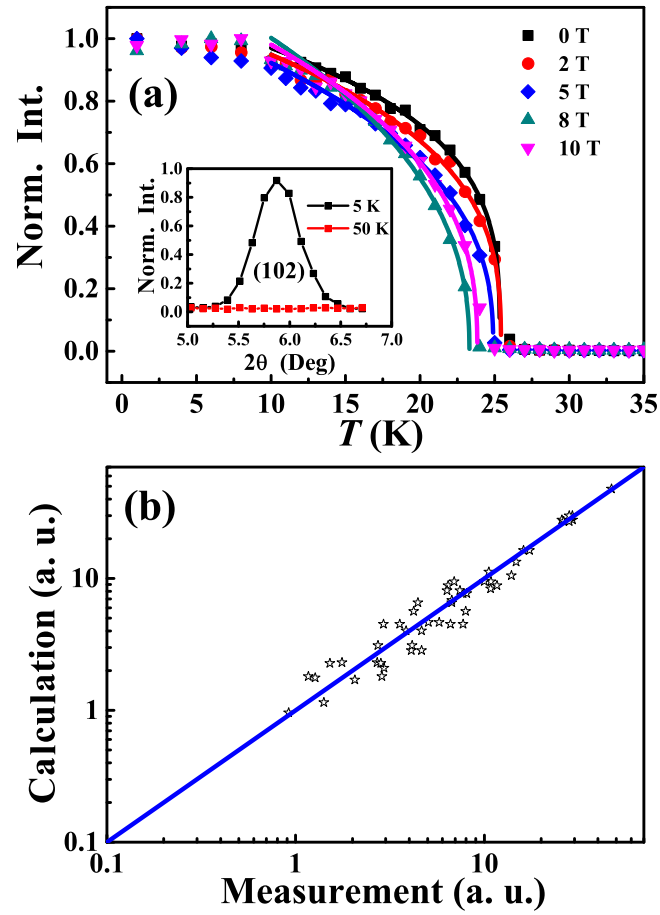

FIG. 5. (a) Temperature dependence of the normalized intensity for the (1 0 2) peak under different magnetic fields. The lines correspond to the power law fits described in the text. Inset: the intensity of the (1 0 2) peak at 5 K and 50 K. The field is applied along the b axis for $BaMn_2Si_2O_7$. (b) The comparison between the observed and calculated F^2 (square magnetic structure factor) for the magnetic reflections.

For $H \leqslant 6$ T along the b axis, the peak (or T_N) shifts to lower temperature with increasing magnetic field. However, the peak position of the $H = 9$ T curve is higher than the 8 T curve, which is consistent with the trend of T_N defined by the magnetic susceptibility. Therefore, the susceptibility, magnetization, and specific heat all consistently exhibit a field-induced spin flop transition around 6 T for $BaMn_2Si_2O_7$, that is similar to the spin flop transition that has been observed in $BaCu_2Si_2O_7$ [12].

To further probe the magnetic properties of $BaMn_2Si_2O_7$, single crystal neutron diffraction measurements were performed under selected temperatures and fields. As shown in the inset of Fig. 5(a), the intensity of the (102) peak appears at 5 K but disappears at 50 K, which represents the antiferromagnetic (AFM) ordering that occurs at lower temperature. The normalized intensities (i.e., the order parameter) for the (102) peak under different magnetic fields are shown in Fig. 5. The T_N shifts to lower temperature with increasing field while $H \leqslant 8$ T and shifts back to a higher temperature for 10 T. The order parameter data can be described by the power law

TABLE I. Crystallographic information, including selected interatomic distances (Å) and bond angle (deg) of $BaMn_2Si_2O_7$ at 5 K.

Crystal symmetry	Monoclinic
Space group	$C2/c$
a (Å)	7.2937
b (Å)	12.9656
c (Å)	13.9819
β (deg)	90.22
V (Å^3)	1327.18
Band	Atomic coordination
Mn-O	Tetrahedral
Si-O	Tetrahedral
Fitted result	Chi^2(Intens): 0.782

function as

$$I = I_0(1 - T/T_N)^{2\beta}, \quad (1)$$

where T_N is the ordering temperature, I_0 is the intensity at base temperature, and β is the order parameter critical exponent. Fitting the data at different magnetic fields [solid lines in Fig. 5(a)] yields values of β ranging from 0.14(8) to 0.21(1), which are slightly smaller than the reported $\beta = 0.22$ from a polycrystalline sample [25].

In total, 53 magnetic Bragg peaks at zero field were measured. The symmetry analysis and refinement based on these peaks determined a spin structure as plotted in Fig. 7(b). In this spin structure, the magnetic moment is along the b axis and has a magnitude of approximately $3.9\mu_B$ at 5 K. The arrangement of the spins along the c and a axes is antiferromagnetic, whereas it is ferromagnetic along the b axis. This spin structure differs from the one reported in the polycrystalline sample study, in which the arrangement of the spin along the a axis is ferromagnetic [25]. Due to the average effect of powder samples, it was difficult to accurately determine the spin structure in our previous study that utilized polycrystalline samples. Therefore, the spin structure obtained from this single crystal using neutron diffraction should represent the true ground state magnetic structure. Moreover, the refinement of the nuclear Bragg peaks yields the crystallographic details presented in Table I. There are some small discrepancies between these results and those reported for polycrystalline samples [25].

B. $BaCo_2Si_2O_7$

The magnetic properties of polycrystalline $BaCo_2Si_2O_7$ ($S = 3/2$) were also investigated. As shown in Fig. 6(a), the temperature dependence of magnetization exhibits a sharp increase below 21 K with $H = 0.01$ T. Meanwhile, the specific heat shows a sharp peak at 21 K in Fig. 6(d). Both results suggest that a long-range magnetic ordering occurs at 21 K. The transition temperature, T_C, is defined as the peak position of the derivative of magnetization (not shown here). As shown in the inset of Fig. 6(a), T_C increases with increasing magnetic field. The hysteresis loop measured at 2 K [Fig. 6(c)] exhibits a square loop that reaches a magnetic moment of $0.3\mu_B$/Co, which is much smaller than the theoretical value $3\mu_B$/Co. The temperature and field dependence of susceptibility and the magnetic loop suggest a weak ferromagnetic ground state for $BaCo_2Si_2O_7$. The linear Curie-Weiss behavior of the inverse susceptibility from 100 to 300 K, as shown in Fig. 6(b), suggests AFM exchange interactions with a Curie temperature $\Theta_{CW} = -58.5$ K. It is interesting that $BaCo_2Si_2O_7$ exhibits weak ferromagnetic ordering but has dominant AFM interactions.

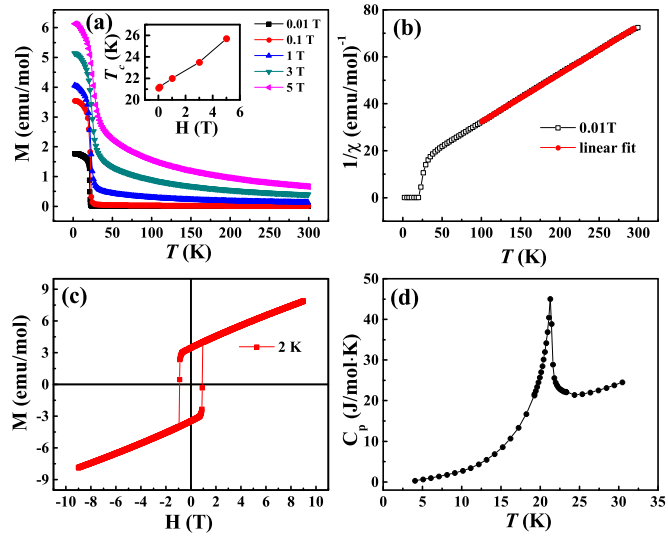

FIG. 6. All data for $BaCo_2Si_2O_7$. (a) The temperature dependence of magnetization under different magnetic fields. (b) The inverse susceptibility measured with $H = 0.01$ T. The squares are experimental data and the solid line is the linear fit. (c) The hysteresis loop measured at 2 K. (d) The temperature dependence of the specific heat. Inset of (a): the field dependence of T_C.

C. LSDA + U calculation

To better understand the exchange interactions in the $BaM_2Si_2O_7$ (M = Cu, Co, and Mn) system, first-principles density-functional theory (DFT) [29,30] calculations have been performed using the LSDA + U method [31] with the Vienna *ab initio* simulation package (VASP) [32]. In this calculation, crystal structures from the references [22,33] were used for the Cu and Co samples, while the crystal structure for the Mn sample was determined from analysis of the single crystal neutron diffraction data in this work. Proper U values, $U = 5.6$ eV [34] for $BaCu_2Si_2O_7$, $U = 7$ eV for $BaMn_2Si_2O_7$, and $U = 5$ eV for $BaCo_2Si_2O_7$, were selected, so that the calculated crystal structures are consistent with the experimental results (see Supplemental Material [35]).

Using the total energies obtained from these calculations, various collinear magnetic configurations are mapped to the Heisenberg model. Magnetic couplings J_i are calculated by linear regression [36]. The equations of regression are given by Hamiltonians of different magnetic structures. For the Cu compound, four interactions, J_a, J_c, J_b, and $J_{[110]}$ or J_{ab} [Fig. 7(a)], have been taken into account. For the Mn and Co compounds, there are three nonequivalent Mn/Co sites due to the lower lattice symmetry. Therefore, the following six interactions have been considered: J_c (M1-M3), J_c (M2-M3), J_a (M1-M2), J_a (M3-M3), J_b, and J_{ab} [Fig. 7(b)]. Equations (2)

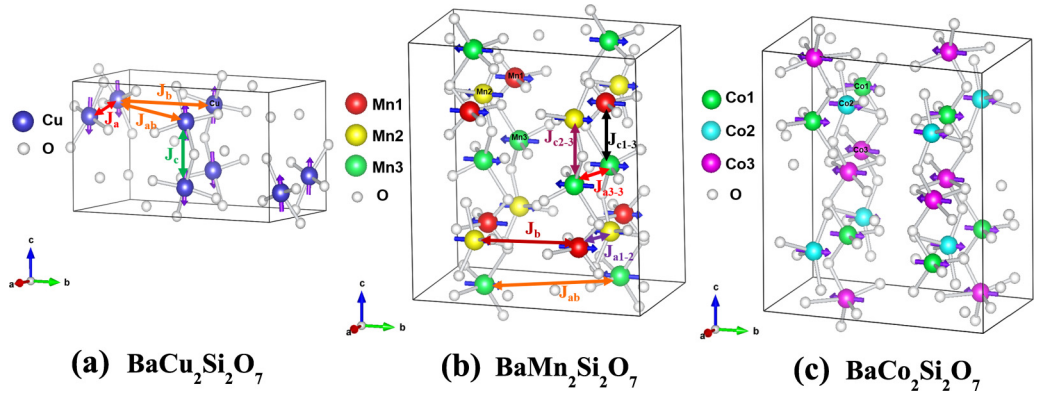

FIG. 7. Schematic superexchange paths and spin structures for $BaM_2Si_2O_7$. The white spheres represent the O^{2-} ions. The arrows represent the spins of M^{2+} ions. The magnetic structure of $BaCu_2Si_2O_7$ was obtained from the Ref. [12]. The magnetic structure of $BaMn_2Si_2O_7$ was obtained from the analyses and refinement of our neutron experiment. The magnetic structure of $BaMn_2Si_2O_7$ was obtained from the Ref. [22] and our magnetization measurement.

and (3) are the Hamiltonians of $M = $ Cu and Co/Mn samples, respectively. In Eq. (3), $n = 9$ or 25 and is the number of possible types of superexchange interactions for the Co and Mn sample, respectively:

$$H_{\mathrm{Cu}} = -\left(\frac{1}{4}J_c\sum_{ij\in c}\vec{s_i}\cdot\vec{s_j}+\frac{1}{4}J_b\sum_{ij\in b}\vec{s_i}\cdot\vec{s_j} + \frac{1}{4}J_a\sum_{ij\in a}\vec{s_i}\cdot\vec{s_j}+\frac{1}{4}J_{ab}\sum_{ij\in ab}\vec{s_i}\cdot\vec{s_j}\right)+H_0, \quad (2)$$

$$H_{\mathrm{Co/Mn}} = -n\left(\frac{1}{4}J_{c_{1-3}}\sum_{ij\in c_1-c_3}\vec{s_i}\cdot\vec{s_j}+\frac{1}{4}J_{c_{2-3}}\sum_{ij\in c_2-c_3}\vec{s_i}\cdot\vec{s_j} + \frac{1}{4}J_b\sum_{ij\in b}\vec{s_i}\cdot\vec{s_j}+\frac{1}{4}J_{a_{1-2}}\sum_{ij\in a_1-a_2}\vec{s_i}\cdot\vec{s_j} + \frac{1}{4}J_{a_{3-3}}\sum_{ij\in a_3-a_3}\vec{s_i}\cdot\vec{s_j}+\frac{1}{4}J_{ab}\sum_{ij\in ab}\vec{s_i}\cdot\vec{s_j}\right)+H_0. \quad (3)$$

There are five noteworthy features of the exchange interactions. (i) The dominating interaction for the Cu sample is $J_c = -17.6$ meV, which is at least two orders of magnitude larger than the other interactions. Most of the obtained interactions from linear regression are quite comparable to those obtained from the mean field theory calculation [11] and experimental spin wave measurement [17], as listed in Table II. One deviation lies with J_b, for which we obtained 0.18 meV and the spin wave simulation led to -0.2 meV. Considering the dominant magnetic couplings in this research, the comparison further validates our calculations. (ii) J_c for the Cu sample is much larger than for the Mn ($J_c = -0.13$ meV) and Co ($J_c = -0.40$ meV) samples. (iii) For the Mn and Co samples, J_c is not significantly larger than J_a and they are comparable on energy scale. (iv) The $J_a = 0.1$ meV for the Co sample shows that is FM, but the Mn sample is AFM as -0.03 and -0.04 meV. (v) For all samples, the J_b and J_{ab} are the weakest interactions.

IV. DISCUSSION

First, we present the magnetic phase diagram for $BaMn_2Si_2O_7$ with H along the b axis, which was constructed by combining the susceptibility, magnetization, heat capacity, and neutron diffraction data, as shown in Fig. 8. At zero field, long-range antiferromagnetic ordering forms below $T_N = 26$ K, which then shifts to lower temperature as the magnetic field increases. Around 6 T, there is a spin flop transition. Because the field applied along the b axis induces the spins to flop perpendicular to the b axis (i.e., possibly in the ac plane) and the magnetization continues to increase

TABLE II. J values (in meV) deduced from the LSDA + U calculations. Negative J represents an AFM interaction and positive J represents a FM interaction.

	$BaCu_2Si_2O_7$		$BaCo_2Si_2O_7$	$BaMn_2Si_2O_7$
	LSDA+U	Mean-field[11] and spin wave[17]	LSDA+U	LSDA+U
J_c	−17.6	−24.1	−0.40(Co3 − Co3) −0.40(Co1 − Co2)	−0.13(Mn3 − Mn3) −0.13(Mn1 − Mn2)
J_b	0.18	−0.2	0.03	0.0002
J_a	0.27	0.46	0.10(Co3 − Co3) 0.10(Co1 − Co2)	−0.03(Mn3 − Mn3) −0.04(Mn1 − Mn2)
J_{ab}	−0.08	−0.15	0.01	−0.0002

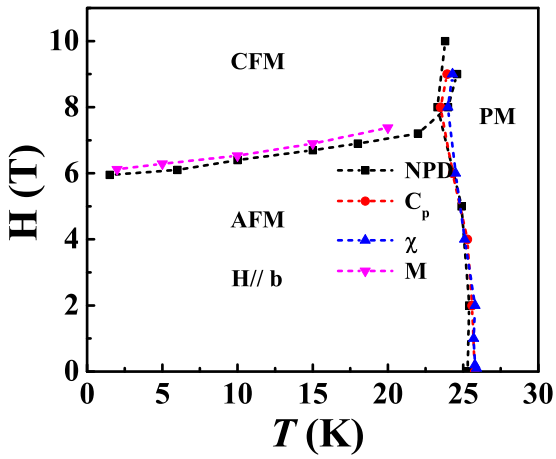

FIG. 8. Magnetic phase diagram for $BaMn_2Si_2O_7$.

linearly between 6 and 9 T, the spin state after the spin flop could be canted state in the *ac* plane. The exact nature of the spin state needs to be studied further. It is noteworthy that a spin flop transition also occurs in $BaCu_2Si_2O_7$ with a smaller critical field of 2 T applied along the *c* axis. As shown in Fig. 7, the spin structure differs from a quasi-1D Cu compound to the 2D Mn compound, which induces a different easy axis of the spin flop that depends on the dimensionality of the sample.

Second, we discuss the magnetic couplings of $BaM_2Si_2O_7$ in detail. The crystal and electronic structures of magnetic atoms cause different interactions. We will analyze the magnetic couplings along the *c* and *a* axes in three samples.

In the Cu sample, the interaction between the nearest Cu^{2+} is through superexchange Cu-O-Cu along the *c* axis but super-superexchange through Cu-O-Si-O-Cu along the *a* axis and Cu-O-Si-O-Si-O-Cu along the *b* axis. Therefore, it is reasonable to see our calculation lead to dominating J_c, which further confirms that the Cu sample is approaching a one-dimensional nature for magnetism.

The fast drop of J_c from Cu to Mn/Co samples could be related to their different outshell electronic configurations. For a Cu^{2+} ion with one half-filled orbital, the interaction along the *c* axis only depends on the superexchange of $3d_{x^2-y^2}(Cu^{2+})$-$p(O^{2-})$-$3d_{x^2-y^2}(Cu^{2+})$. For a Mn^{2+} ion, its five half-filled 3*d* orbitals split to three high energy t_{2g} and two low energy e_g orbitals due to the MnO_4 tetrahedral site. All five orbitals can involve superexchange interaction through $p(O^{2-})$ orbitals with orbitals in another Mn^{2+} ion, which results in 25 combinations of superexchange in the Mn compound. Since the bond angles 121.9° for Mn3-O1-Mn2 and 105.22° for Mn1-O4-Mn3 along the *c* axis are between 90° and 180°, each interaction of these 25 combinations is determined by the competition between ferromagnetic and antiferromagnetic superexchange nature according to GKA rules [37]. Then it is possible that this competition can compensate each other within the possible interactions and lead to a significant decrease of the total J_c interaction. For a Co sample with isostructure to a Mn sample, there are only three half-filled 3*d* orbitals, which can lead to a smaller magnitude of J_c.

The structural distortion in the Mn/Co sample has another consequence: the ratio between the M-M bond length along the *c* and *a* axes is smaller than that for the Cu sample. Moreover, the J_c is reduced in the Mn/Co sample and is comparable to J_a, hence making the Mn/Co sample approaches of a two-dimensional nature in magnetism. The higher dimension of Mn/Co samples induces higher magnetic ordering temperatures than that of a Cu compound. Although Mn and Co samples had the isostructure, the magnetic ground states are different—AFM and ferrimagneticlike, respectively. This difference reflected in our calculation demonstrated the different nature of J_a, which is AFM for Mn but FM for the Co compound. The Co^{2+} ion has no half filled e_g orbitals involving the interactions, while the Mn^{2+} ion has two half filled e_g orbitals. Since the interactions involving these e_g orbitals along the *a* axis favor AFM, the total interactions of the Co sample are still under competition between AFM and FM. Furthermore, the reduction of the AFM interaction with the lack of half filled e_g orbitals can lead to a final FM nature of the total interaction for the Co sample. Finally, the spin structure for the Co sample shows FM along the *a*- and *b*-axis AFM along the *c* axis. The calculation assumed the collinear spins; this calculated spin structure of the Co sample could be slightly different from the experimental result. While its true spin structure needs further neutron measurements to be confirmed, the magnetization measurements on single crystal samples [22] suggested that the spins are canted along the *c* axis with a small angle around 5° and this canting should be the origin for its weak ferromagnetism.

To further elaborate this interesting difference between Mn and Co samples, we looked into the monoxide MnO and CoO samples, which are a NaCl structure with the M^{2+} (M = Co/Mn) ion on the MO_6 octahedral site. The nearest interaction in MnO is AFM [38], while the nearest interaction in CoO is FM [39]. When analyzing MnO and CoO similar to the analysis of $BaX_2Si_2O_7$ (X = Co, Mn) present here, the results are qualitatively the same.

V. CONCLUSION

In summary, we constructed a magnetic phase diagram and obtained a more accurate antiferromagnetic spin structure for single crystalline $BaMn_2Si_2O_7$ by performing susceptibility, magnetization, specific heat, and single crystal neutron diffraction measurements. We also confirmed the weak ferromagnetism of polycrystalline $BaCo_2Si_2O_7$. Finally, in order to systematically understand the different magnetic ground states in the $BaM_2Si_2O_7$ (M = Cu, Co, and Mn) system, we performed LSDA + U calculations and extracted the magnetic exchange interactions. Our discussions based on the comparison among the exchange interactions suggest that the different crystal structure and the orbital effect on the interaction are the main reasons for the changes of magnetic properties from Cu to Co and to Mn samples.

ACKNOWLEDGMENTS

This work is supported by the National Natural Science Foundation of China (NSFC) with Grants No. 11774223, No. 11474197, No. U1632272, No. 11521404, and No. 11574201. J.M., G.H.W., and H.D.Z. acknowledge the support from the Ministry of Science and Technology of China (Grants No. 2016YFA0300500 and No. 2016YFA0301003). A portion

of this research used resources at the High Flux Isotope Reactor, a DOE Office of Science User Facility operated by the Oak Ridge National Laboratory. Q.H. acknowledges the support from the GO! Student Program of ORNL. H.D.Z. also acknowledges the support from NSF-DMR with Grant No. NSF-DMR-1350002. D.Q. acknowledges support from the Changjiang Scholars Program. Computations were performed at the HPC of Shanghai Jiao Tong University, China. We also acknowledge Michael Koehler for polishing the manuscript.

[1] E. Ising, Z. Phys. **31**, 253 (1925).
[2] W. Heisenberg, Z. Phys. **49**, 619 (1928).
[3] N. D. Mermin and H. Wagner, Phys. Rev. Lett. **17**, 1133 (1966).
[4] Y. J. Kim, M. Greven, U.-J. Wiese, and R. J. Birgeneau, Eur. Phys. J. B **4**, 291 (1998).
[5] R. B. Griffiths, Phys. Rev. **133**, A768 (1964).
[6] J. C. Bonner and M. E. Fisher, Phys. Rev. **135**, A640 (1964).
[7] M. Takahashi, Prog. Theor. Phys. **46**, 401 (1971).
[8] M. Takahashi and M. Suzuki, Prog. Theor. Phys. **48**, 2187 (1972).
[9] I. S. Jacobs, J. W. Bray, H. R. Hart, L. V. Interrante, J. S. Kasper, G. D. Watkins, D. E. Prober, and J. C. Bonner, Phys. Rev. B **14**, 3036 (1976).
[10] S. Eggert, I. Affleck, and M. Takahashi, Phys. Rev. Lett. **73**, 332 (1994).
[11] I. Tsukada, Y. Sasago, K. Uchinokura, A. Zheludev, S. Maslov, G. Shirane, K. Kakurai, and E. Ressouche, Phys. Rev. B **60**, 6601 (1999).
[12] I. Tsukada, J. Takeya, T. Masuda, and K. Uchinokura, Phys. Rev. Lett. **87**, 127203 (2001).
[13] A. Zheludev, E. Ressouche, I. Tsukada, T. Masuda, and K. Uchinokura, Phys. Rev. B **65**, 174416 (2002).
[14] V. Glazkov and H.-A. Krug von Nidda, Phys. Rev. B **69**, 212405 (2004).
[15] V. Glazkov, G. Dhalenne, A. Revcolevschi, and A. Zheludev, J. Phys.: Condens. Matter **23**, 086003 (2011).
[16] A. Zheludev, M. Kenzelmann, S. Raymond, E. Ressouche, T. Masuda, K. Kakurai, S. Maslov, I. Tsukada, K. Uchinokura, and A. Wildes, Phys. Rev. Lett. **85**, 4799 (2000).
[17] M. Kenzelmann, A. Zheludev, S. Raymond, E. Ressouche, T. Masuda, P. Boni, K. Kakurai, I. Tsukada, K. Uchinokura, and R. Coldea, Phys. Rev. B **64**, 054422 (2001).
[18] A. Zheludev, M. Kenzelmann, S. Raymond, T. Masuda, K. Uchinokura, and S. H. Lee, Phys. Rev. B **65**, 014402 (2001).
[19] R. Hayn, V. A. Pashchenko, A. Stepanov, T. Masuda, and K. Uchinokura, Phys. Rev. B **66**, 184414 (2002).
[20] A. Zheludev, S. Raymond, L. P. Regnault, F. H. L. Essler, K. Kakurai, T. Masuda, and K. Uchinokura, Phys. Rev. B **67**, 134406 (2003).
[21] R. D. Adams, R. Layland, T. Datta, and C. Payen, Polyhedron **12**, 2075 (1993).
[22] R. D. Adams, R. Layland, C. Payen, and T. Datta, Inorg. Chem. **35**, 3492 (1996).
[23] G. X. Lu, L. Q. Yang, and J. H. Lin, Solid State Commun. **114**, 113 (2000).
[24] M. Akaki, F. Nakamura, D. Akahoshi, and H. Kuwahara, Phys. B **403**, 1505 (2008).
[25] J. Ma, C. D. Dela Cruz, T. Hong, W. Tian, A. A. Aczel, S. X. Chi, J. Q. Yan, Z. L. Dun, H. D. Zhou, and M. Matsuda, Phys. Rev. B **88**, 144405 (2013).
[26] B. C. Chakoumakos, H. Cao, F. Ye, A. D. Stoica, M. Popovici, M. Sundaram, W. Zhou, J. S. Hicks, G. W. Lynn, and R. A. Riedel, J. Appl. Crystallogr. **44**, 655 (2011).
[27] J. Rodríguez-Carvajal, Physica B **192**, 55 (1993).
[28] R. Dingle, M. E. Lines, and S. L. Holt, Phys. Rev. **187**, 643 (1969).
[29] P. Hohenberg and W. Kohn, Phys. Rev. **136**, B864 (1964).
[30] W. Kohn and L. J. Sham, Phys. Rev. **140**, A1133 (1965).
[31] A. I. Liechtenstein, V. I. Anisimov, and J. Zaanen, Phys. Rev. B **52**, R5467 (1995).
[32] G. Kresse and J. Furthmuller, Phys. Rev. B **54**, 11169 (1996).
[33] T. Yamada, Z. Hiroi, and M. Takano, J. Solid State Chem. **156**, 101 (2001).
[34] S. Bertaina and R. Hayn, Phys. Rev. B **73**, 212409 (2006).
[35] See Supplemental Material at http://link.aps.org/supplemental/10.1103/PhysRevB.100.035131 for how we chose the U value.
[36] M. Toyoda, K. Yamauchi, and T. Oguchi, Phys. Rev. B **87**, 224430 (2013).
[37] J. B. Goodenough and A. L. Loeb, Phys. Rev. **98**, 391 (1955); J. B. Goodenough, J. Phys. Chem. Solids **6**, 287 (1958); J. Kanamori, *ibid.* **10**, 87 (1959); P. W. Anderson, Phys. Rev. **115**, 2 (1959).
[38] G. Pepy, J. Phys. Chem. Solids **35**, 433 (1974).
[39] K. Tomiyasu and S. Itoh, J. Phys. Soc. Jpn. **75**, 084708 (2006).